

Finite Element Analysis of Thorax Responses Under Quasi-Static and Dynamic Loading

Jikuang Yang, Fang Wang, Guibing Li, and Xiaoqing Jiang

Abstract This study aimed at investigation of the response of the human thorax under various loading conditions. For this purpose an FE thorax model was developed based on the human anatomical structures. The human thorax consists of ribs, thoracic vertebrae and intervertebral discs, a sternum, costal cartilages and internal organs. Material properties used in this study were based on the published literature. The FE model was used to simulate the phenomenon of thorax compression. The simulations were carried out in different configurations, including the three-point bending of single rib and frontal impacting with a cylinder to a complete thorax at low speed. The results from simulations were compared with the impact responses obtained from biological tests, such as 3-point bending tests and rib structural tests. The entire thorax model was then tested by simulation of volunteer test. The responses predicted by the simulation showed a good biofidelity.

1 Introduction

Thorax injuries are often observed in vehicle traffic accidents. The number of fatalities and serious injuries ranked the second in reported passenger vehicle crashes [1]. It is also indicated that thoracic injuries occurred in vehicle–pedestrian collisions, especially for collisions with MPV and mini bus. It is therefore necessary to have a good understanding of the thoracic injury mechanism to reduce the injury risk in vehicle accidents. The dynamic responses and injury mechanisms

J.K. Yang (✉)

State Key Laboratory of Advanced Design and Manufacturing for Vehicle Body, Hunan University, Changsha, China

Department of Applied Mechanics, Chalmers University of Technology, Sweden

e-mail: jikuang.yang@chalmers.se; jikuangyang@hnu.edu.cn

F. Wang • G.B. Li • X.Q. Jiang

State Key Laboratory of Advanced Design and Manufacturing for Vehicle Body, Hunan University, Changsha, China

have been widely studied by using biological material, mechanical dummies, and mathematical model. Recent years, many studies have carried out by using human body FE models for dynamic responses and injury mechanisms of the thorax in frontal or lateral loading [2]. An FE model of the 50th percentile adult males was developed by Emmanuel Lizee et al. for predicting dynamic responses of a driver in car frontal and side impact [3]. In a study by Gordon R. Plank et al. [4], a coupled FE model of the human thorax with a Hybrid III dummy (replaced Hybrid III thorax) was used in simulations of an out-of-position driver during airbag deployment. Shah et al. [5] used a human thorax FE model [6] developed by Wang to predict modes of loading that are most likely to produce aortic ruptures. Jesse et al. [7] developed a full human model to simulate the human thoracic dynamic responses and injuries associated with frontal impact, side impact, and belt loading.

Since 1997 the EC funded the HUMOS and HUMOS2 [8,9] projects developed a series of FE human models with aims at prediction of injury risks for victims involved in road traffic accidents. In addition, TOYOTA developed a series FE models (THUMS) of human body in order to estimate injuries in traffic accidents involved occupant and pedestrian [10].

The aim of this study was to simulate dynamic responses of the thorax and rib fractures under different load conditions by using an FE human thorax model developed at Hunan University based on the anatomical structures [11, 12].

2 Method and Materials

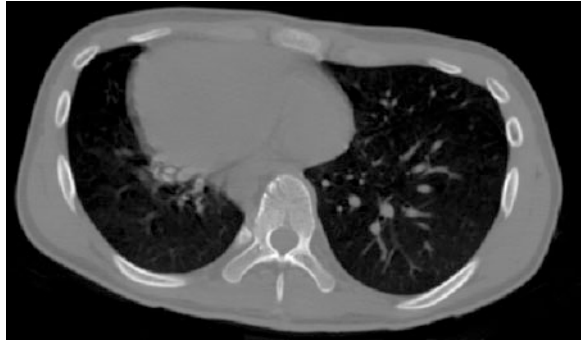
An FE thorax model was developed based on a mid-size adult male. Basic geometry data of the thorax model was based on medical data. The validity of the model was evaluated by simulation of the experimental tests using biological specimens. The solver for the simulation used here is LS-DYNA with the Hyperworks as the pre & post-processor. A study was carried out for understanding of the thorax responses to low speed collisions.

2.1 *Anatomy-Based Human Thorax FE Model*

Basic geometry data of the human thorax FE model was based on computed tomography (CT) scanner sections of a lying individual from a medical university, the subject is average in size and in weight. Each slice was 1 mm thick. Figure 1 shows a slice of the intermediate sternum location.

The thorax FE model consists of ribs, thoracic vertebrae and intervertebral discs, a sternum, costal cartilage and internal organs. Each rib is different in length, shape, and orientation, and the ribs are classified as true (1–7), false (8–10) or floating (11–12). True ribs connect between the vertebrae and sternum; false ribs connect

Fig. 1 Image for the anatomic data of thorax



between the vertebrae and the rib immediately above it; and floating ribs connect only to the vertebrae.

The thoracic vertebra body consists of outer cortical bone and the inner cancellous bone. The cortical bone was modeled as isotropic elastic plastic material using shell elements while the cancellous bone was modeled as the same material using 8-node solid elements. Each intervertebral disc composes of nucleus pulpous (NP) and its surrounding components—annulus fibrosus (AF). They were all represented with 8-node solid elements.

The ribs, costal cartilages, and the sternum were modeled in the same way as thoracic vertebra; outer cortical bone modeled using shell elements while the cancellous bone modeled using 8-node solid elements.

The soft tissues filling in the ribcage, the abdomen and the pelvis cavity are also represented in the model. The different organs, like the heart, spleen, lung, stomach, liver, and intestines, were modeled with solid elements; the muscles and adipose tissues covering the ribcage and the abdominal organs were represented by a layer of solid elements and a layer of shell elements.

There are several spinal ligaments and muscles. All of the ligaments were modeled with bi-linear spring elements that can only carry loads in tension and the muscles were modeled with beam elements. Figure 2 shows the frontal and back views of the FE human thorax model.

2.2 Material Properties

The material models for the skeleton structure were considered as either elastic-plastic or linear elastic. In the modeling of the internal organs, the linear visco-elastic material law (LS-DYNA material type MAT_06) was used. The visco-elastic law defined by a compressibility module k and a relaxation function in shear:

$$G(t) = G_0 + (G_0 - G_i)^* \exp(-\beta t), \quad (1)$$

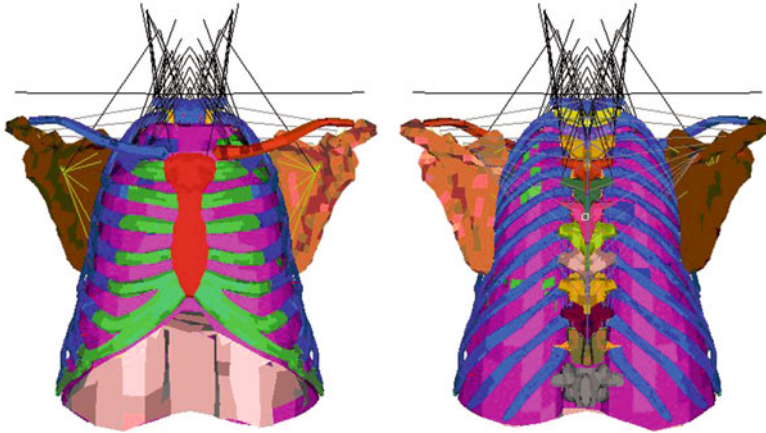


Fig. 2 The frontal (L) and dorsal (R) views skeleton of the FE human thorax model

Table 1 Material definition of the model skeleton components

	Material Model	Density (kg/m^3)	E (MPa)	Poison Ratio	Yield Stress (MPa)	K (MPa)	Reference
Vertebra solid	Elastic	2,500	11,000	0.3	–	–	[13]
Vertebra shell	Elastic	2,500	100	0.3	–	–	[7]
Disc Nucleus Pulposus	Elastic	1,040	2,300	0.3	–	–	[7]
Disc Anulus Fibrosus	Elastic	1,040	300	0.3	–	–	[7]
Sternum trabecular	Elastic	1,000	0.05	0.3	–	–	[7]
Sternum cortical	Elastic	2,000	9,600	0.3	–	–	[7]
Rib Cartilage trabecular	Elastic	1,000	70	0.3	–	–	[13]
Rib Cartilage cortical	Elastic-Plastic	2,000	49	0.3	4.84	15.6	[13]
Rib trabecular	Elastic-Plastic	1,000	40	0.3	1.8	32	[14]
Rib cortical	Elastic-Plastic	2,000	10,000	0.3	90	1,800	[7]

E = Young's modulus, k = bulk modulus

where G_0 = short-term shear modulus, G_i = long-term shear modulus, β = decay constant.

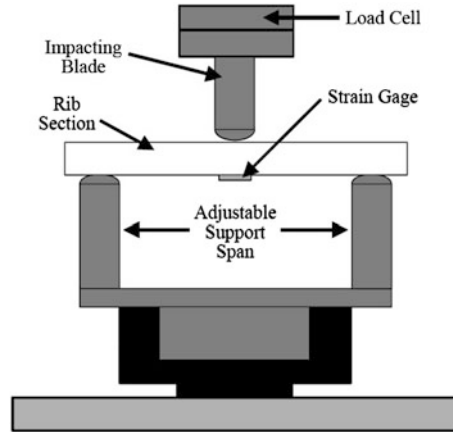
All of the material parameters used in the current model is given in Tables 1 and 2.

Table 2 Material definition of the model soft tissues component

Tissues	Material Model	Density kg/m ³	k (MPa)	Shear Modulus			β (decay constant)	Reference
				G ₀ (MPa)	G _i (MPa)	G _i (MPa)		
Heart	Vi-elastic	1,000	8.3	0.00384	0.001	0.001	0.25	Wang [6];
Lungs	Vi-elastic	1,000	3.333	0.00715	0.00415	0.00415	0.25	
Spleen	Vi-elastic	1,000	0.25	0.054	0.04	0.04	0.25	Stephane [9];
Liver	Vi-elastic	1,000	0.166	0.045	0.036	0.036	0.25	
Kidney	Vi-elastic	1,000	0.166	0.045	0.036	0.036	0.25	Jesse et al. [7];
Stomach	Vi-elastic	1,000	0.25	0.054	0.04	0.04	0.25	
Intestine	Vi-elastic	1,000	0.025	0.036	0.027	0.027	0.25	Jay and Gopal [13]

k = bulk modulus

Fig. 3 Apparatus used for human rib three-point bending



2.3 Simulation of Rib Fracture

Rib fractures are common thoracic injuries that can result in mortality and severe morbidity. For good understanding of biomechanical properties of the human rib, a large number of experiments have been performed using cadaver rib specimens—including shearing tests [15], 3-point bending tests [15–19], and tension coupon tests [20]. Based on the test data, the material properties, such as the elastic modulus, yield stress, yield strain, ultimate stress, and ultimate strain were determined within certain ranges from the resulting stress versus strain curves. In 1976 Granik and Stein performed on 10 human rib specimens from the 6th and 7th ribs. Afterwards more experimental studies [17–19] were conducted using cadaver specimens of different ribs by other researchers. Of all the rib tests, attention was paid to the 3-point bending properties. Strain was measured by placing a strain gage at the center of the tension side of the rib section. The Young's modulus was calculated by using linear elastic beam equations.

Kallieris et al. [21] investigated the correlation between rib deflection and applied force by performing 3-point bending quasi-static and dynamic tests on the 6th and 7th ribs obtained from PMHSs as presented in Fig. 3. Each rib specimen was placed on between two supports with distance 0.1 m. Rib specimens were loaded till the material failure at velocities of 2 m/s and 4 m/s in the dynamic tests and at 0.02 m/s in quasi-static tests. The 3-point bending tests were simulated with FE models of the ribs from ribcage of the thorax model. According to the configuration in Kallieris tests the impactor was modeled as a rigid sphere with a radius equal to 0.013 m and a weight of 2.35 kg. The cortical failure strains are defined based on the strain rate from literature [22].

Zuoping Li et al. [22] performed quasi-static noninjurious (0.002 m/s for all) and dynamic injurious (1 m/s for R2 and 0.5 m/s for L4 and L10) experiments using the 2nd, 4th, and 10th human rib to record the structural behavior and fracture tolerance of individual ribs under anterior–posterior bending loads as seen in frontal

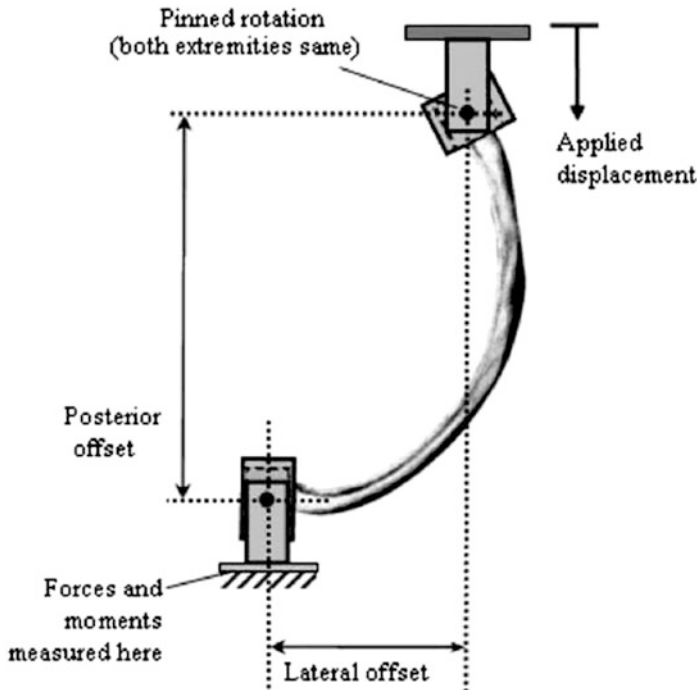


Fig. 4 Setup of rib structural test [22]

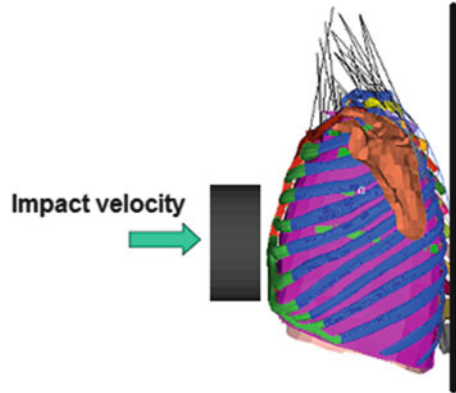
impact, which demonstrated in Fig. 4. Reaction forces at the posterior extremity, the displacement time history at the anterior extremity, and the cortical bone strain were measured.

In the simulation study, the configuration of FE rib model was defined based on the setup of the experimental loading and boundary conditions [22] in the corresponding rib structural test (Fig. 4). The anterior and posterior extremities were modeled by spherical FE joints with free rotation permitted in the loading plane only. The displacement of anterior extremity was prescribed at a constant velocity equal to those applied during the experiments. The resultant joint force at the posterior extremity was output for comparison with the measured reaction forces for each rib.

2.4 Whole Thorax FE Model Simulation

Many frontal blunt impact tests have been conducted to determine the force-deflection corridors of the human chest. It has been suggested that blunt impacts are a better test method when assessing the stiffness of the chest compared to sled tests [13]. In the 1970s a total of 35 frontal chest pendulum impact tests

Fig. 5 Initial condition for hub loading



have been conducted [23, 24]. In these tests, the subjects were positioned in a sitting posture on a flat surface of a rigid table with a free-back configuration. The impactor was centered on the sternum in the mid-sagittal plane at the level of the fourth intercostals space and the load was delivered by an unpadded flat wooden impactor with rounded edges and a diameter of 152 mm. These tests were analyzed by Neathery [25, 26]. There was also another series of experiments performed by Patrick [27] at Ford. In Patrick's tests, the volunteer was fixed-back and the posterior of the chest movement was essentially zero during the tests. A cylinder simulating a steering wheel hub (diameter: 152 mm, mass: 10 kg) impacted to the anterior surface of the thorax of a volunteer at an initial velocity of 3.4–4.6 m/s. Each test was synchronized on high-speed film and the displacement of the impactor and the forces by load cell were measured to calculate force-deflection curves.

In this study the entire thorax model was simulated according to Patrick's tests. Figure 5 shows the setup of simulation of thoracic impactor test performed by Patrick [27].

The force-deflection response was reconstructed by using the thorax model under every initial speed in the tests (initial velocity: 3.4 m/s for 3 times, 4.2 m/s and 4.6 m/s for 1 time). The impactor force was output as a contact load between the impactor surface and the anterior surface of the thorax. Impactor displacement was calculated from node displacement, and thoracic deflection was calculated from changes in the distance between nodes on the anterior and posterior surfaces of the thorax.

3 Results

3.1 Analysis of the Rib Fractures

The force-deflection histories from quasi-static, low rate, and high rate (Fig. 6-abc) loading simulations were plotted against the experimental corridors achieved by Kallieris [21].

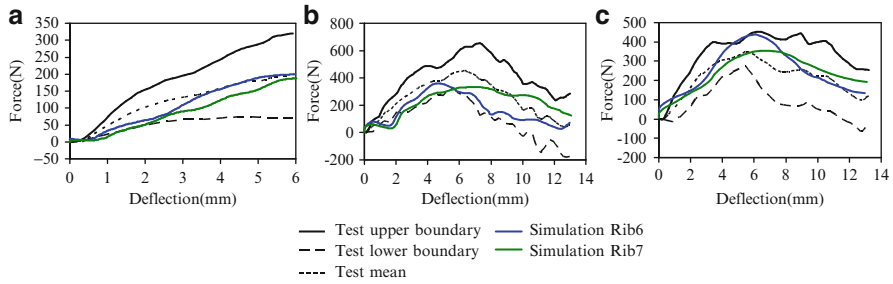


Fig. 6 Three-point bending loading simulation comparing with Kallieris tests. (a) Quasi-static 0.02 m/s, (b) Dynamic 2 m/s, (c) Dynamic 4 m

Table 3 Static and dynamic results from experiments (Exp) and FE simulation (Sim) for the 2nd, 4th, and 10th ribs

Subject	Model	Static Data		Dynamic Data	
		Displacement (mm)	Resultant Reaction force (N)	Fracture Time (ms)	Resultant Reaction force (N)
419m-Rib 2R	Exp	10	57.1	18.9	90.7
	Sim	10	72.8	22.0	143.7
413m-Rib 4L	Exp	14	51.9	82	123.4
	Sim	14	46.8	102.3	128.0
412m-Rib 10L	Exp	16	41.2	122	87.6
	Sim	16	40.5	120.8	96.1

In simulation of the rib 3-point bending tests (Fig. 6), the forces after reaching their maximum value show a decreasing tendency due to fracture of the rib in dynamic tests which finds a good agreement with the test. It is possible that the material of the cortical bone is modeled with a damage model, and applying a damage model with failure parameters allowed showing the ribs fracture, and consequently, more biofidelic force-deflection curves would be obtained. Meanwhile in the quasi-static test simulation, the force increases with the deflection within the range showed in the literature, just like the test output. In dynamic test simulations the ribs' material strain rate dependency also could be demonstrated.

Differences are seen when comparing the computational and experimental resultant reaction force of the rib structural static tests [22] as well as the fracture time and the reaction force at the fracture moment of the structural dynamic tests [22] as shown in Table 3.

The force-displacement curves of the structural test simulation with second, fourth, and tenth rib FE model comparing with the test data under dynamic loading are shown in Fig. 7. It could be seen that in the simulation of the ribs at different velocities, the results represent almost the same tendency as in the test. Also, the differences of rib fracture time between simulations and tests in the comparison curves reflect what is shown in Table 3.

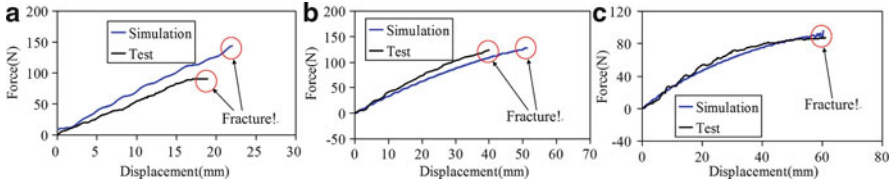


Fig. 7 The structural loading simulation comparing with the Zuoping Li tests. (a) Rib2 at 1 m/s, (b) Rib4 at 0.5 m/s, (c) Rib10 at 0.5 m/s

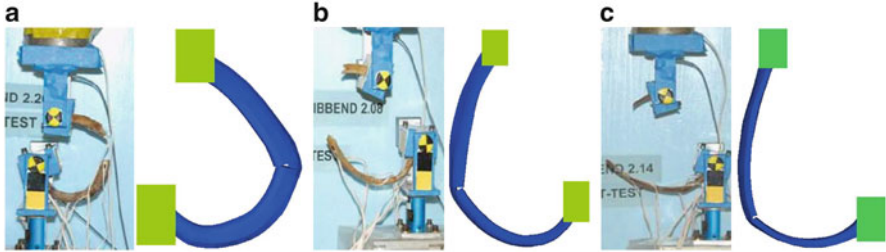


Fig. 8 The rib fracture locations of simulations comparing with the Zuoping Li tests. (a) Rib2 at 1 m/s, (b) Rib4 at 0.5 m/s, (c) Rib10 at 0.5 m/s

Figure 8 compares the fracture locations between the FE simulations and Zuoping Li et al. [22] tests under dynamic loading conditions. The FE models predict closer fracture locations to the posterior extremity of the rib bone than that of the experimental locations, it is considered due to that there are some age-dependent differences in material properties of human body tissues among the subjects from which the experimental bony sections and the FE model geometry are obtained, which is also reported by Zuoping Li et al. [22] and Qing Zhou et al. [28]. Moreover, the variation of the rib cortical thickness, the accuracy of the cortical geometry captured, and the material properties chosen for the FE model also have effect on the biomechanical responses [21, 29].

3.2 Results of the Thorax FE Model Simulation

Figure 9 shows the observed state of the thoracic geometry after impactor contact at the highest velocity of 4.6 m/s, it shows the thoracic deflection of 0 mm, 20 mm, 40 mm and 60 mm. In this case, maximum thoracic deflection was 59.8 mm, which is also shown in Fig. 10c.

The following results are based upon the limited number of impact simulation and range of velocities.

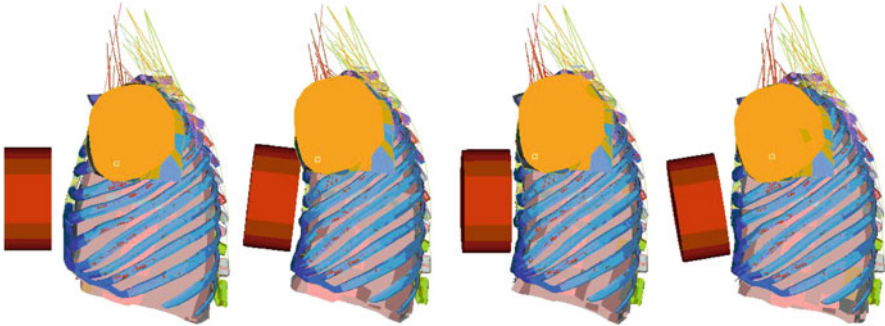


Fig. 9 Kinematics of the thorax model for a 4.6 m/s frontal chest impact with a 10 kg mass pendulum

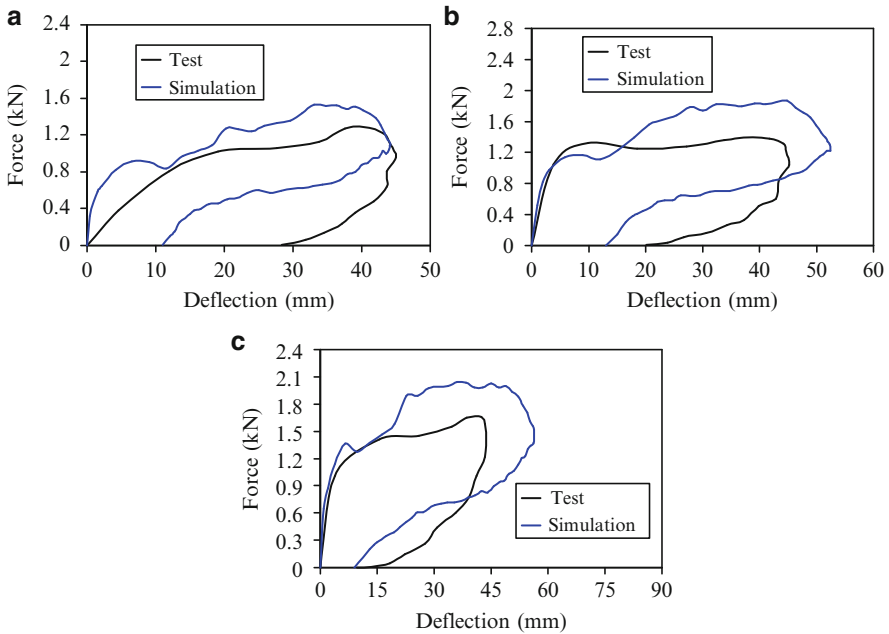


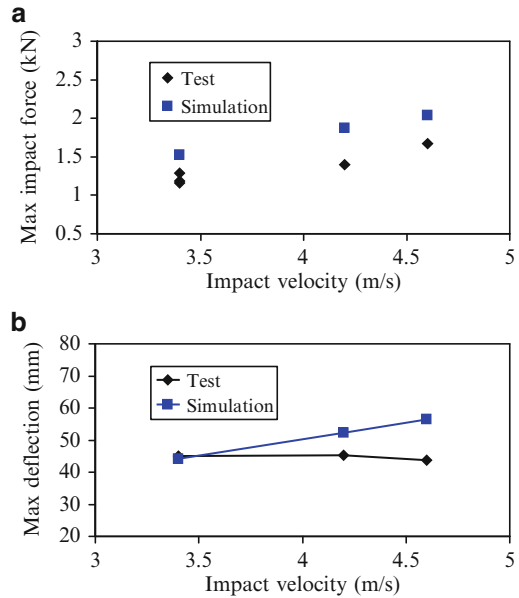
Fig. 10 The comparison of force-deflection time history curves between test and simulation. (a) 3.4 m/s (b) 4.2 m/s (c) 4.6 m/s

In the test, force increases initially with deflection, reaches an initial peak or plateau before continuing up to a maximum peak, but the same phenomenon was not so distinctly represented in the simulation results (Fig. 10).

The maximum force of 2.03 kN occurred at the maximum impact velocity of 4.6 m/s in simulations and that is 1.67 kN at 4.6 m/s in the tests (Figs. 10 and 11a).

The maximum deflection of the impact varies linearly with impact velocities based on the simulation, which does not agree with the test result. Actually, the

Fig. 11 The comparison of peak values between test and simulation. (a) force vs. impact velocity (b) deflection vs. impact velocity



maximum chest compression in the tests was essentially the same, 4.37–4.57 cm (Figs. 10 and 11b).

The maximum force of the impact varies linearly with impact velocities based on the simulation, which agreed with the test result (Fig. 11a).

4 Discussions

The human rib FE models were used to simulate the 3-point bending tests performed by Kallieris et al. [21] and the structural quasi-static and dynamic tests carried out by Zuoping Li et al. [22]. The former simulation results well reflect the test data and the latter results just obtain an acceptable agreement with the results from structural tests. There are some factors causing the differences between the results of the simulations and tests, which would also be the focus of coming research.

For simulations of the frontal pendulum impact, the maximum impact force predicted by the FE model was 22%–34% higher than that obtained from experiments. While the maximum deflection as a function of impact velocity was not exactly the same as that of the tests. The maximum chest compression in the tests was essentially the same (Figs. 10 and 11b), but based on the simulation the maximum deflection of the impact varies linearly with impact velocities. Moreover, it is very difficult to imagine that during the analysis of the Patrick tests [27], discrepancies were found when comparing the initial energy with the integrated energy of the force-displacement curves. It is therefore necessary and important to obtain more

information about the tests and adjust the responses of the human thorax FE model to determine the fidelity of the correlations. However, giving the viscoelasticity and strain rate dependency of the human bone material, it seems like that the simulation results make more sense.

The number of the volunteer tests reported in the literature is limited. The material constitutive laws and material properties chosen in this study were, in general, consistent with previous studies designed to develop the 50th percentile male models. For the reason, various scaling and compromising methods, mainly on the material properties, have been used on the model.

Among the experimental results available in the literature, different authors reported many rib fractures. In order to account for this phenomenon, a failure plastic strain is introduced in the rib material law. More research is also needed to increase the accuracy of predictability for thoracic injuries so that the human chest injury mechanisms can be better understood.

5 Conclusions

The simulations of dynamic response of the human thorax under impact load were carried out by using an FE human thorax model based on the anatomical structures. This model includes a detailed description of the bony skeleton, chest, and abdominal internal organs.

The responses predicted by the rib model matched reasonably well with experimental data obtained from rib three-point bending tests and rib structural tests. The whole thorax simulation of a series of hub loading volunteer tests showed some discrepancy comparing with the test results. The model is expected to be applied for the injury prediction of rib fractures under the reported loading conditions in biological tests.

References

1. Shin, J., Untaroiu, C., Lessley, D. et al.: Thoracic Response to Shoulder Belt Loading: Investigation of Chest Stiffness and Longitudinal Strain Pattern of Ribs. Society of Automotive Engineers, SAE 2009-01-0384 (2009)
2. Yang, K.H., Hu, J.W., White, N.A. et al.: Development of numerical models for injury biomechanics research: a review of 50 Years of Publications in the Stapp Car Crash conference. 50th Stapp Car Crash J. 50, 429-490 (2006)
3. Lizee, E., Rohin, S., Song, E. et al.: Development of a 3D Finite Element Model of the Human Body. Society of Automotive Engineers, SAE 983152 (1998)
4. Plank, G.R., Kleinberger, M., Eppinger, R.H.: Analytical Investigation of Driver Thoracic Response to Out of Position Airbag Deployment. Society of Automotive Engineers, SAE 983165 (1998)
5. Shah, C.S., Yang, K.H., Hardy, W. et al.: Development of a Computer Model to Predict Aortic Rupture Due to Impact Loading. Society of Automotive Engineers, SAE 2001-22-0007 (2001)

6. Wang, H-C.: Development of a side impact finite element human thoracic model, Doctoral Dissertation, Wayne State University, US, 1995.
7. Ruan, J., EI-Jawahri, R., Li, C. et al.: Prediction and analysis of human thoracic impact responses and injuries in cadaver impacts using a full human body finite element model. 47th Stapp Car Crash J. **47**, 299–321 (2003)
8. Vezin, P., Verriest, J.P.: Development of a set of numerical human models for safety. In: Proceedings of the 19th International Technical Conference on the Enhanced Safety of Vehicles, Washington D.C, US, Paper No. 05–0163 (2005)
9. Robin, S.: HUMOS: human model for safety – a joint effort towards the development of refined human-like car occupant models. In: Proceedings of the 17th International Technical Conference on the Enhanced Safety of Vehicles, Amsterdam, The Netherlands, Paper No. 01 - 0297 (2001)
10. Iwamoto, M., Kisanuki, Y., Watanabe, I. et al.: Development of a finite element model of the total human model for safety (THUMS) and application to injury reconstruction. In: Proceedings of the International Research Council on the Biomechanics of Impacts (IRCOBI) Conference, Munich, Germany, pp. 31–42 (2002)
11. Yang, J.K., Xu, W., Otte, D.: Brain injury biomechanics in real world vehicle accident using mathematical models. Chin. J. Mech. Eng. **32**(4), 81–86 (2008)
12. Yang, J.K., Yao, J.F.: Development and validation of a human neck FE model in impact loading condition. J. Hunan Univ. Natural Sci. **30**, 40–46 (2003) (In Chinese)
13. Zhao, J., Narwani, G.: Development of a human body finite element model for restraint system R&D application. In: Proceedings of the 19th International Technical Conference on the Enhanced Safety of Vehicles, Washington D.C, US, Paper No. 05 - 0399 (2005)
14. Kimpara, H., Lee, J.B., Yang, K.H. et al.: Development of a three-dimensional finite element chest model for the 5th percentile female. 49th Stapp Car Crash J. **49**, 251–269 (2005)
15. Sacreste, J., Brun-Cassan, F., Fayon, A. et al.: Proposal for a thorax tolerance level in side impacts based on 62 tests performed with cadavers having known bone condition. 26th Stapp Car Crash J. 155–171 (1982)
16. Stein, I.D., Granik, G.: Rib structure and bending strength: an autopsy study. Calcif. Tissue Int. **20**, 61–73 (1976)
17. Stitzel, J.D., Cormier, J.M., Barretta, J.T. et al.: Defining regional variation in the material properties of human rib cortical bone and its effect on fracture prediction. 47th Stapp Car Crash J. **47**, 243–265 (2003)
18. Cormier, J.M., Stitzel, J.D., Duma, S.M. et al.: Regional variation in the structural response and geometrical properties of human ribs. In: Proc. 49th Association for the Advancement Automotive Conference, Boston, US, pp. 153–170 (2005)
19. Yoganandan, N., Pintar, F.A.: Biomechanics of human thoracic ribs. J. Biomech. Eng. **120**, 100–104 (1998)
20. Kemper, A.R., McNally, C., Kennedy, E.A., et al.: Material properties of human rib cortical bone from dynamic tension coupon testing. 49th Stapp Car Crash J. **49**, 199–230 (2005)
21. Kallieris, D., Schonpflug, M., Yang, J. et al.: Report on Injury Mechanisms Database/Version B (2004)
22. Li, Z., Kindig, M.W., Subit, D. et al.: Influence of mesh density, cortical thickness and material properties on human rib fracture prediction. Med. Eng. Phys. **32**, 998–1008 (2010a)
23. Kroell, C.K., Schneider, D.C., Nahum, A.M.: Impact tolerance and response of the human thorax. 15th Stapp Car Crash J. 84–134 (1971)
24. Kroell, C.K., Schneider, D.C., Nahum, A.M.: Impact tolerance and response of the human thorax . 18th Stapp Car Crash J. 383–457 (1974)
25. Neathery, R.F.: Analysis of chest impact response data and scaled performance recommendations. 18th Stapp Car Crash J. 459–493 (1974)
26. Kent, R., Lessley, D., Sherwood, C.: Thoracic response to dynamic, non-impact loading from a hub, distributed belt, diagonal belt, and double diagonal belts. 48th Stapp Car Crash J. 495–519 (2004)

27. Patrick, L.M.: Impact force-deflection of the human thorax. 25th Stapp Car Crash J. 471–496 (1981)
28. Zhou, Q., Rouhana, S.W., Melvin, J.W.: Age effects on thoracic injury tolerance. 40th Stapp Car Crash J. 137–148 (1996)
29. Li, Z., Kindig, M.W., Kerrigan, J.R. et al.: Rib fractures under anterior-posterior dynamic loads: experimental and finite element study. *J. Biomech.* **43**(2), 228–324 (2010b)